Polarization-rich continuous wave direct imaging: modeling and visualization

AQ:A

R. S. Umesh, A. G. Ramakrishnan, R. Srikanth, R. Hema, and S. Divya

We report a study and comparison of continuous-wave, optical polarization difference imaging (PDI) and polarization modulation imaging (PMI) for imaging through scattering media. The problem is cast in the framework of a theoretical estimation, and the comparison is based on three visualization parameters, namely, the magnitude, the degree, and the orientation of the polarization. We show that PDI is superior in estimating the first two parameters in active imaging under specific conditions, while the PMI is suitable for passive imaging and is the only way to estimate polarization orientation. We also propose new schemes for rendering polarization information as a color image and for applying the newly introduced polarization-orientation imaging for segmentation. Simulation and experimental results verify the theoretical conclusions.

OCIS codes: 290.0290, 110.7050, 110.2990, 170.4580.

1. Introduction

In direct optical imaging, the sole aim is to use only unscattered light for imaging.[1] The criteria for rejecting and accepting different parts of the radiation as scattered and unscattered vary and give rise to different imaging schemes. In this study we consider only continuous-wave, direct imaging schemes that use linear polarization of the received radiation to discriminate the unscattered from the scattered part of the radiation. Part of this study was reported earlier.[2] Here we extend our earlier study and report new imaging and visualization schemes and applications. From this study, parallels can be drawn with the case of circular polarization.

In many schemes one subtracts sets of copolarized and cross-polarized images or their scaled versions to obtain the image that corresponds to the unscattered component of light[3,4] and hence belong to the class of polarization difference imaging (PDI). There are other schemes that use polarization modulation followed by sinusoidal estimation[5,6] and achieve the same goal. These schemes belong to the category of polarization modulation imaging (PMI). These schemes are used to measure either the intensity of polarized light [polarization intensity imaging (PII)],[5,6] or the degree of linear polarization[7] (DOLP) of the received radiation.[3,4] PDI has been shown to be capable of measuring these parameters.[3,4] PMI has been used only for PII, although, as we show, it can also be used for estimating the DOLP and for estimating the orientation of a linearly polarized source. Further, PDI is useful for both active and passive imaging, whereas PMI, described in Refs. 5 and 6, is useful only for active imaging.

However, we can make PMI suitable for both active and passive imaging by keeping the plane of polarization of the incident light fixed and allowing the analyzer to rotate. Then we can observe that PDI becomes a particular case of this modified PMI scheme if images are captured at angular displacements of $\pi/2$ of the analyzer. The frequency of the sinusoid that results from unscattered light will be half the sampling rate; i.e., only two points of the sinusoid will be sampled per period. If one of the sampled points (images) is chosen to be at the maximum of the sinusoid (the copolarized image), the next sample will be at the minimum of the sinusoid (the cross-polarized image). Thus we can get PDI data by properly choosing the sampling point in the modified PMI scheme. Hence PDI is a particular case of the more versatile PMI. Henceforth, all references to PMI will essentially refer to this modified PMI scheme. Using PMI schemes we can estimate polarization orientation (PO) information by estimating the phase of the received sinu-

R. S. Umesh (umeshrs@ee.iisc.ernet.in), A. G. Ramakrishnan, and R. Srikanth are with the Department of Electrical Engineering, Indian Institute of Science, Bangalore 560 012, India. R. Hema and S. Divya are with the Optics Laboratory, Raman Research Institute, Bangalore 560 012, India.

Received 8 July 2005; accepted 15 November 2005; posted 17 January 2006 (Doc. ID 63291).

0003-6935/06/180001-11$15.00/0

soid, which can be achieved with PII data. This visualization parameter is useful for isolating various linearly polarized sources that may exist in a scene. We identify the corresponding imaging as polarization orientation imaging (POI).

2. Signal Modeling

As we observed, it is sufficient to model the data obtained by PMI because we can easily obtain PDI data from the same data. We model the observed data (images obtained) by using the Stokes vectors (SVs).[7–9] In general, the SVs recorded at a pixel location of a CCD camera by use of any polarization-based optical imaging can be represented as $|\langle I_s\rangle \langle Q_s\rangle \langle U_s\rangle \langle V_s\rangle|'$, where $\langle\,\rangle$ represents the spatiotemporal averaging over the CCD pixel area for a period equal to the integration time of the CCD. We make a realistic assumption that the CCD integration times are usually large compared with the coherence times of the sources,[10] and hence, by virtue of the central limit theorem, the spatiotemporally averaged SVs recorded during different subintervals can be assumed to be Gaussian independent and identically distributed (iid) random variables.[10]

Though this assumption seems reasonable for most of the experimental data collected, in some cases data revealed an underlying colored noise that could be adequately modeled by an autoregressive noise, AR1. Hence in our model we do not assume that the noise is white. By Malus's law,[9] if light with SV $S_{in} = [I_s Q_s U_s V_s]^T$ is incident onto a linear polarizer whose polarization axis subtends an angle θ from the horizontal, the intensity of the output SV is related to the input parameters by

$$I_o = \tfrac{1}{2}(I_s + Q_s \cos 2\theta + U_s \sin 2\theta). \tag{1}$$

Thus the intensity recorded at an arbitrary pixel location at the nth step of acquisition of PMI can be represented as

$$I_r(n) = \tfrac{1}{2}(I_s + Q_s \cos 2\theta_n + U_s \sin 2\theta_n) + v(n),$$
$$n = 0, \ldots, N-1, \tag{2}$$

where θ_n is the angle made by the analyzer with respect to the horizontal at the nth step and $v(n)$, in general, represents colored noise. Assuming that the rotating polaroid takes M steps to complete exactly one rotation, θ_n is incremented by $2\pi c/M$ with each step of the polaroid. Suppose that we start grabbing images with an arbitrary orientation ϕ of the rotating polaroid. Then the intensity recorded at the nth step can be represented as

$$I_r(n) = \frac{1}{2}\left[I_s + \sqrt{Q_s^2 + U_s^2}\,\sin\left(\frac{4\pi n}{M} + 2\phi + \alpha\right)\right] + v(n), \tag{3}$$

where $\alpha = \arctan(Q_s/U_s)$.

We observe from Eq. (3) that the component of the intensity that is independent of the orientation of the analyzer is $I_s/2$, which corresponds to the diffuse part of the scattered light. The amplitude of the sinusoidal part, i.e., $(Q_s^2 + U_s^2)^{1/2}/2$, corresponds to the unscattered component that would be polarized and hence is a measure of the magnitude of the polarized light in the received radiation. We denote the former I_{scat} and the latter I_{bal}. Using this representation we find that

$$I_r(n) = I_{scat} + I_{bal}\sin\left(\frac{4\pi n}{M} + \beta\right) + v(n),$$
$$n = 0, \ldots, N-1, \tag{4}$$

where we have replaced the term $2\phi + \alpha$ by a single variable, β. The discrete frequency f of I_{bal} is given by $f = 2/M$.

In all our comparisons of the imaging schemes, we assume that there are N images (N even and $\gg M$) available for analysis; i.e., for PDI there would be $N/2$ images each, corresponding to the copolarized and the cross-polarized data. In PMI schemes there would be N images constituting a time series at every pixel location, which would be analyzed for estimating the sinusoidal component. We further assume that N is an integral multiple of M (however, this condition is not strict for N large). A comparison of the analysis schemes needs knowledge of the noise statistics at each pixel location, which are seldom known *a priori*. Still, we assume that the noise characteristics are known and analyze the various schemes because we get an idea of the performance of the various estimators given a particular noise condition. We do not explicitly estimate the noise variance terms, as the quantity of interest to us is the unscattered component of light and noise is a nuisance parameter. We now compare PDI and PMI, based on this model.

The comparative studies of all the imaging schemes have been separated into two cases. First we treat white noise and then, colored noise. More often than not, when the noise is white we get simple closed-form solutions for the bounds on the performance of imaging schemes, thereby allowing an easy comparison to be made across schemes. This simplicity is seldom found when the noise is colored because then we have to resort to numerical simulations. Thus we are encouraged to have a separate study when the noise is white. We have maintained this pattern throughout this study.

3. Polarization Intensity Imaging

A. White Noise

1. PDI Estimator

We denote the copolarized intensity recorded in a general PDI scheme $I_{\parallel}$ and the cross-polarized intensity $I_{\perp}$. As the plane of polarization of the incident

light is not known in general, these intensities need not correspond to the exact copolarization and cross-polarization locations. We assume that the intensity recorded with the analyzer at an angle ϕ with respect to the horizontal is I_ϕ. Thus the recorded copolarized and cross-polarized intensities will be [from Eq. (4)]

$$I_{\parallel}(n) = I_{\text{scat}} + I_{\text{bal}} \sin(\beta) + w(n), \tag{5}$$

$$I_{\perp}(n) = I_{\text{scat}} + I_{\text{bal}} \sin(\beta + \pi) + w'(n), \tag{6}$$

where $w(n)$ and $w'(n)$ are zero mean iid Gaussian random variables and $\beta = (2\phi + \alpha)$. Using PDI, we can obtain the estimate of the unscattered component in the recorded data as

$$\hat{I}_{\text{bal,PDI}} = \frac{1}{N} \sum_{n=1}^{N/2} [I_{\parallel}(n) - I_{\perp}(n)]. \tag{7}$$

In some implementations of PDI, the scaling factor is an arbitrary constant.[3,11] However, the correct theoretical estimate of the unscattered component is given only by Eq. (7). Now, by substituting the expressions for $I_\parallel$ and $I_\perp$ from Eqs. (5) and (6) into Eq. (7), and by simplifying the resultant expression, we obtain

$$\hat{I}_{\text{bal,PDI}} = I_{\text{bal}} \sin \beta + w^*(n), \tag{8}$$

where $w^*(n)$ is a zero mean, Gaussian iid noise, with variance σ^2/N, where σ^2 is the variance of $w(n)$ and $w'(n)$. We can observe from Eq. (8) that

$$E\{\hat{I}_{\text{bal,PDI}}\} = I_{\text{bal}} \sin \beta, \tag{9}$$

$$\text{var}\{\hat{I}_{\text{bal,PDI}}\} = \sigma^2/N. \tag{10}$$

Clearly, the estimate $\hat{I}_{\text{bal,PDI}}$ is biased because the estimated value depends on β. This is a big disadvantage of PDI. Only when $\beta = \pi/2$ do we get the true estimate of the unscattered component. The estimator has a variance of σ^2/N, irrespective of the value of β. Next we analyze the performance of the PMI polarization intensity estimator.

2. PMI Estimator

Suppose that N data values from PMI are available for analysis. It can be observed from Eq. (4) that the $2N/M$th component of the N-point discrete fourier transform would contain information on the sinusoid. The estimate of I_{bal} is given by

$$\hat{I}_{\text{bal,PMI}} = \frac{2}{N} \left| \Pi\left(\frac{2N}{M}\right) \right|, \tag{11}$$

AQ:E where Π is the discrete Fourier transform of $I_r(n)$ of Eq. (4).

Here again, some PMI schemes use a different scaling factor.[5] The analysis of the bias and variance of this estimator is quite complex, and hence we have resorted to numerical simulations. We compare the results of the simulation with that of the PDI intensity estimator below. Next we analyze what best can be done to estimate I_{bal} from PMI data, from the basic principles of estimation theory.

The best estimator, with the optimality criteria being that the estimator should be unbiased and should possess minimum variance, is known to be the minimum variance, unbiased (MVU) estimator.[12] To determine whether a MVU estimator exists, we need to see whether some estimator satisfies the Cramer–Rao lower bound (CRLB). Here the quantity that we wish to estimate is I_{bal} of Eq. (4). However, it can easily be found that a MVU estimator does not exist for I_{bal} using PMI. Hence we resort to estimating the maximum-likelihood estimator (MLE) of I_{bal}, as the MLE is known to be asymptotically efficient and optimal. Moreover, if an efficient estimator exists, it will be achieved by the MLE.[12]

The problem on hand is similar to estimating the amplitude of a single sinusoid, except for the constant term I_{scat}. We explore whether we can extend the analysis of the case of a single sinusoid[12] to that of ours. It is clear that by modifying Eq. (4) as given below we can modeled the data linearly as

$$I_r(n) = I_{\text{scat}} + I_{\text{bal}} \cos \beta \sin\left(\frac{4\pi n}{M}\right) + I_{\text{bal}} \sin \beta \cos\left(\frac{4\pi n}{M}\right) + w(n),$$

$$n = 0, \ldots, N-1. \tag{12}$$

With this modification, we can express Eq. (12) as

$$\underbrace{\begin{bmatrix} I_r(0) \\ I_r(1) \\ I_r(2) \\ \vdots \end{bmatrix}}_{\mathbf{I}_r} = \underbrace{\begin{bmatrix} 1 & 0 & 1 \\ 1 & \sin(4\pi/M) & \cos(4\pi/M) \\ 1 & \sin(8\pi/M) & \cos(8\pi/M) \\ \vdots & \vdots & \vdots \end{bmatrix}}_{\mathbf{H}} \underbrace{\begin{bmatrix} I_{\text{scat}} \\ I_{\text{bal}} \cos \beta \\ I_{\text{bal}} \sin \beta \end{bmatrix}}_{\boldsymbol{\Theta}} + \underbrace{\begin{bmatrix} w(0) \\ w(1) \\ w(2) \\ \vdots \end{bmatrix}}_{\mathbf{W}}, \tag{13}$$

or, with matrix notation, as

$$\mathbf{I}_r = \mathbf{H}\boldsymbol{\Theta} + \mathbf{W}. \tag{14}$$

If we can estimate $I_{\text{bal}} \cos \beta$ and $I_{\text{bal}} \sin \beta$, we can estimate I_{bal}. It has been proved that, for data represented in a linear form as above, the MLE of $\boldsymbol{\Theta}$ is[12]

$$\hat{\boldsymbol{\Theta}} = (\mathbf{H}^T\mathbf{C}^{-1}\mathbf{H})^{-1}\mathbf{H}^T\mathbf{C}^{-1}\mathbf{I}_r, \tag{15}$$

where $\mathbf{C}$ is the noise covariance matrix.

$\hat{\boldsymbol{\Theta}}$ is also an efficient estimator, in that it attains the CRLB and hence is the MVU estimator. Thus we have efficient estimators for $I_{bal} \cos \beta$ and $I_{bal} \sin \beta$, and thus the MLE for I_{bal} (Ref. 12) is given by

$$\hat{I}_{bal,MLE} = +[(I_{bal} \cos \beta)^2 + (I_{bal} \sin \beta)^2]^{1/2}. \quad (16)$$

Although I_{bal} is biased if data points are few, it is asymptotically unbiased.[13] Moreover, as the estimate is obtained by a nonlinear transformation of the MVU estimates, the estimator cannot be efficient.[12] From Eq. (15), the MLE $\hat{\boldsymbol{\Theta}}$ for various components can be shown to be

$$\hat{I}_{scat,MVU} = \frac{1}{N} \sum_{n=0}^{N-1} I_r(n), \quad (17)$$

$$\hat{I}_{bal} \cos \beta_{MVU} = \frac{2}{N} \sum_{n=0}^{N-1} I_r(n) \sin\left(\frac{4\pi n}{M}\right), \quad (18)$$

$$\hat{I}_{bal} \sin \beta_{MVU} = \frac{2}{N} \sum_{n=0}^{N-1} I_r(n) \cos\left(\frac{4\pi n}{M}\right), \quad (19)$$

$$\mathrm{var}\{\hat{I}_{scat,MVU}\} = \frac{\sigma^2}{N}, \quad (20)$$

$$\mathrm{var}\{\hat{I}_{bal} \cos \beta_{MVU}\} = \mathrm{var}\{\hat{I}_{bal} \sin \beta_{MVU}\} = \frac{2\sigma^2}{N}. \quad (21)$$

From Eq. (18) and Eq. (19) it can be inferred that the right-hand side of Eq. (16) is the same as that of Eq. (11). Hence we arrive at the important result that the MLE estimate of I_{bal} can be obtained by PMI. It is worth observing that, if $\beta = \pi/2$, we can obtain the MVU estimates of I_{bal}. Hence, if we know the exact orientation of the plane of polarization of the source, we can obtain the MVU estimates of I_{bal} by PMI. We end our search for better estimators of I_{bal} here, because the MLE almost always does the best job when the MVU estimator does not exist.

The exact phase relations can usually be known in the case of active imaging. Hence, for active imaging, PDI schemes are more useful than PMI. For passive imaging, PMI seems to be more suitable. However, there are applications for which the parameter of interest is not the exact value of the sinusoidal amplitude but its relative value across the scene. Because PDI gives uniformly scaled values of the sinusoidal amplitude across the scene, it may be better to use PDI in such circumstances, as its variance is lower than that of PMI. With this, we conclude our analysis of the estimators for I_{bal} in white noise.

B. Colored Noise

The theoretical analysis of the estimators in colored noise is a formidable task, and hence we have resorted to Monte Carlo simulations with which to compare the estimators. However, a few important observations can be made before we procede to the results. For the same reasons as for white noise, it has been found that we cannot obtain a MVU estimate of I_{bal} by PMI, and we have to be satisfied with the MLE given by Eq. (15). However, what makes colored noise different is that noise covariance matrix $\mathbf{C}$ in this case will not be $\sigma^2\mathbf{I}$, and hence the estimates depend explicitly on the terms of the covariance matrix. On the other hand, if the noise is white, we can obtain the MLEs of the amplitude without having to know the noise variance *per se*. Usually, we do not get the noise samples alone because the data contain signal plus noise information. This makes the estimation of the noise covariance matrix difficult. Hence numerous estimators have been designed to tackle this problem.[13]

Among the matched-filter based estimation techniques,[13] for our application the amplitude and phase estimator for sinusoids (APES) algorithm seems to be the best suited, because we need to estimate the amplitude of one sinusoid only. We now compare the estimation results obtained from the PDI and PMI estimates and the APES, as used for the data generated by use of Monte Carlo simulations.

C. Results from Monte Carlo Simulations

Simulations to test the PMI and MLE estimators and the APES used 200 instances of 64 data points generated according to Eq. (4), with signal frequency f assumed to be 0.125. For testing the PDI estimator we used 32 data points each, with $\beta = \pi/2, 3\pi/2$, corresponding to the copolarized and the cross-polarized data, respectively. The values of I_{scat} and I_{bal} are chosen to be 4 and 1, respectively, so the DOLP corresponds to 0.25. We observed that the performance of the estimators does not depend on the actual values of I_{scat} or I_{bal} but on the signal-to-noise ratio (SNR).

We studied various characteristics of the estimators by varying the SNR through the variance of the iid Gaussian random variable that governs noise.[13] For deciding the range of SNR values to be considered we calculated the average SNR of a 10×20 region of eight data sets that we obtained experimentally. Such an analysis showed the actual SNR to vary from approximately -14 dB to 9 dB. Hence we have considered a SNR range from -25 to $+25$ dB for our analysis. Though we found that the noise in the actual data could be adequately represented by autoregressive noise AR1. We tested the algorithms with AR2 noise too, so the performance of the estimators in unknown noise conditions could be better understood. For studying the performance of the estimators during AR1 noise, we chose AR coefficient a to be 0.50 in all the simulations. To study the performance of the estimators in AR2 noise we chose the AR coefficients to be $a_1 = 0.50$ and $a_2 = -0.125$. The pole frequency for this choice of AR coefficients corresponds to a discrete frequency of 0.125 and coincides with the frequency of the sinusoid, thus creating a

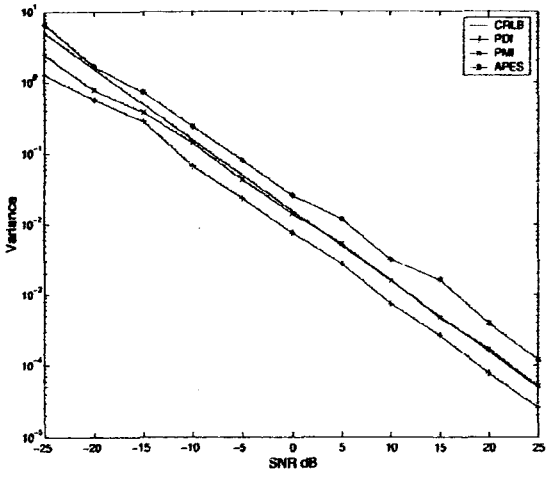

(a)

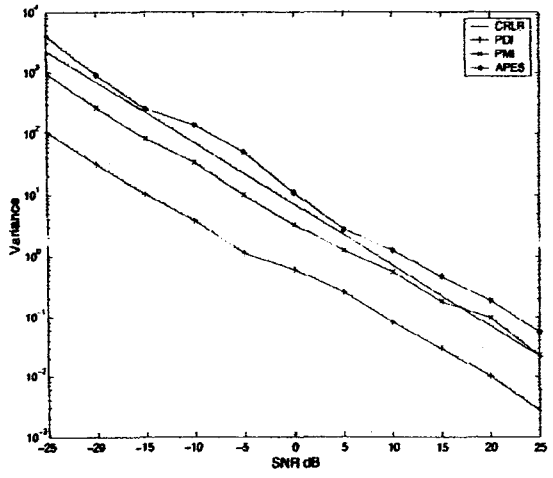

(b)

Fig. 1. Performance of PII estimators. (a) Variance of PII estimators in white noise. (b) Variance of PII estimators in AR1 noise.

relatively difficult situation in which to estimate the sinusoidal amplitude.

The performance of all the estimators was similar in AR1 and AR2 noise conditions. Hence we do not report our observations of the performance of the estimators in AR2 noise. Moreover, the bias of the estimators has not been reported because β was chosen to be $\pi/2$, so all the estimators were unbiased and behaved in the expected manner. Further, given that the relative values of the parameters, and not the absolute values, are what are usually sought, the variance becomes a more important criterion in choosing an estimator than its bias. Hence in all further comparisons (including other imaging schemes and noise characteristics), we report only the variance of the various estimators and not their bias.

Figures 1(a) and 1(b) show the performance of the various estimators in white and colored noise, respectively. We can observe that PDI and PMI perform consistently better than the APES estimator. Though PMI and the MLE are one and the same in this case (and hence are not distinctly shown), the high computational cost of implementing the MLE favors the use of PMI implementation. As can be observed, to implement the MLE we need to wait to store data until the last data sample is obtained, unlike in the PMI, which can be implemented in place sequentially by use of Goertzel's and similar algorithms. PDI exhibits less bias and variance (at $\beta = \pi/2$), verifying our theoretical observations. It can be observed that the variance of the PDI estimator for both white and AR1 noise and the PMI estimator in AR1 noise are below the CRLB. These results are not unexpected, because the estimators will be biased under these circumstances.

4. Degree of Polarization Imaging

An imaging scheme that uses the DOLP as the visualization parameter is reported;[3] the DOLP is defined as

$$\mathrm{DOLP} = \frac{I_{\parallel} - I_{\perp}}{I_{\parallel} + I_{\perp}}. \tag{22}$$

$I_{\parallel}$ and $I_{\perp}$ refer to the copolarized and cross-polarized intensities, respectively. Substituting $\beta = \pi/2$ into Eqs. (5) and Eq. (6) and in the absence of noise, we obtain

$$\mathrm{DOLP} = \frac{I_{\mathrm{bal}}}{I_{\mathrm{scat}}} = \frac{\left[Q_s^{\,2} + U_s^{\,2}\right]^{1/2}}{I_s}. \tag{23}$$

Two estimators that represent the extreme cases of the general estimator described above are

$$\widehat{\mathrm{DOLP}}_{\mathrm{PDI1}} = \frac{\sum_{n=0}^{\langle N/2\rangle-1}\left[I_{\parallel}(n) - I_{\perp}(n)\right]}{\sum_{n=0}^{\langle N-2\rangle-1}\left[I_{\parallel}(n) + I_{\perp}(n)\right]}, \tag{24}$$

$$\widehat{\mathrm{DOLP}}_{\mathrm{PDI2}} = \frac{2}{N}\sum_{n=0}^{\langle N/2\rangle-1}\left[\frac{I_{\parallel}(n) - I_{\perp}(n)}{I_{\parallel}(n) + I_{\perp}(n)}\right]. \tag{25}$$

Here, we have assumed that N is even, for mathematical convenience, though this is not a necessary condition. It is clear that all the estimators derived from Eq. (24) will be biased, because the numerator corresponds to scaled versions of the polarization intensity data, which were shown to be biased. However, if $\beta = \pi/2$ in Eq. (5) and Eq. (6), or if the relative (rather than the actual) values of the DOLP in a scene are of interest, then $\widehat{\mathrm{DOLP}}_{\mathrm{PDI}}$ can be used. However, if $\beta \to 0$, the noise may completely obscure the DOLP information. Henceforth we shall assume that $\beta = \pi/2$, so the numerator is an unbiased estimate of I_{bal}. The form of $\widehat{\mathrm{DOLP}}_{\mathrm{PDI}}$ is that of a ratio estimator, with both the numerator and the denominator being Gaussian random variables that are uncorrelated if the noise is white but correlated for colored noise. A comparative study of these estimators has been reported in Ref. 14. It has been found that the $\widehat{\mathrm{DOLP}}_{\mathrm{PDI2}}$

estimator is biased and that $\widehat{DOLP}_{PDI1}$ is asymptotically unbiased. The variances of the estimators are equal and diminish to zero asymptotically. Hence both estimators are consistent. For these reasons it is better to use $\widehat{DOLP}_{PDI1}$. It can also be observed that the memory requirements of $\widehat{DOLP}_{PDI1}$ are less than those of $\widehat{DOLP}_{PDI2}$.

A. PMI Estimator of the DOLP

In our analysis of PII we found that, for $\beta \neq \pi/2$, we can obtain only the MLE of I_{bal} and not its MVU estimate. We can show that the MLE of I_{scat} also corresponds to its MVU estimate in both colored and white noise. Hence we can obtain the MLE of the DOLP by using the invariance property of the MLE.[12] As the transformation $\widehat{DOLP} = \hat{I}_{bal}/\hat{I}_{scat}$ is noninvertible, the MLE maximizes a modified likelihood function, as explained in Ref. 12. From the theorem on the asymptotic behavior of the MLE,[12] we conclude that the MLE achieves the CRLB asymptotically.

B. Results from Monte Carlo Simulations

F2 Figures 2(a) and 2(b) show the performance of the various estimators in white and AR1 noise, respectively. We can observe that PDI and PMI estimators seem to be the best for estimating the DOLP too, with PDI performing better than PMI (with $\beta = \pi/2$). It can be observed that, for AR1 noise, meaningful conclusions about the behavior of the estimators can be arrived at only at values of the SNR above 5 dB. Hence, in general, the performance of the estimators is poor for colored noise. As can be observed, the variance of the PDI estimator is lower than the CRLB, as is not unexpected, given that the estimator is biased if $\beta \neq \pi/2$.

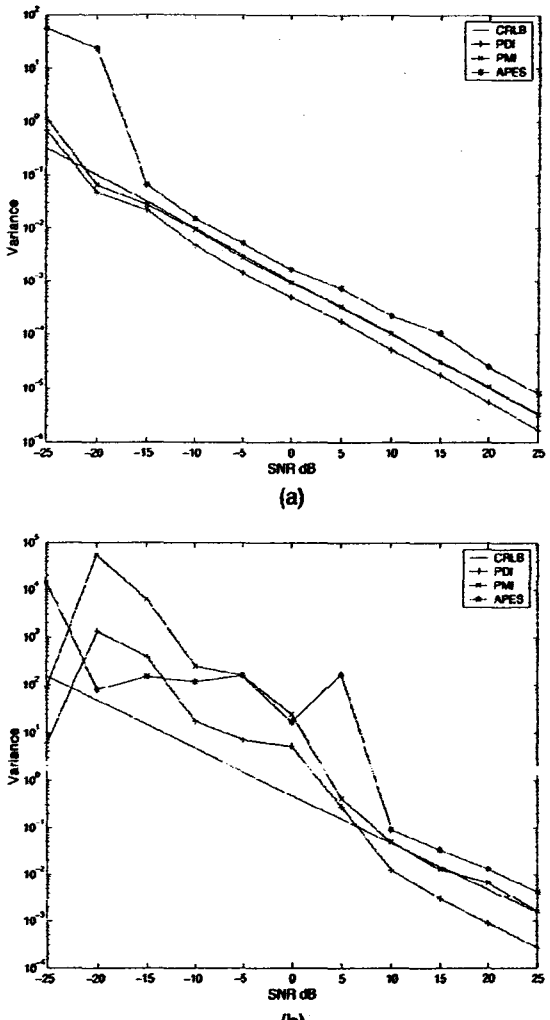

Fig. 2. Performance of DOLP estimators. (a) Variance of DOLP estimators in white noise. (b) Variance of DOLP estimators in AR1 noise.

5. Polarization Orientation Imaging

The received radiation can contain different states of linear polarization for various reasons. It could be due to extraneous polarized sources deployed for other imaging purposes. It could also be due to changes in the polarization state induced by reflection. The latter case is more commonly encountered in passive imaging situations, for which specular surfaces can change the orientation of the plane of polarization of incident linearly polarized light or can even induce polarization in the incident unpolarized light. In any case, the ability to distinguish different states of linear polarization adds value to the imaging AQ: J methodology. Further, as we show below, this can be obtained with the data obtained with the existing PMI schemes.

Assume that a PMI experiment is conducted with arbitrary orientation of the plane of polarization of the source, yielding data that follow Eq. (4). With all the parameters the same, we study the effect on the recorded data of a change in the orientation of the plane of polarization of the source by an angle γ.

For Eq. (3) we assumed that angle ϕ represents the orientation of the rotating polaroid with respect to the horizontal. Now we need to replace ϕ by $\phi + \gamma$. This change essentially leads to a change in the value of β, which corresponds to the change in phase of the recorded sinusoids; i.e., a change in the orientation of the plane of polarization manifests itself as a change in the phase of the recorded sinusoids and does not affect the sinusoidal and dc amplitudes.

PII and DOLP imaging cannot capture this information, as they ignore the estimated phase of the sinusoids, even though all the estimators except the PDI estimator can give this information. Thus we can use the same estimators to obtain all three visualization parameters, namely, polarization intensity, DOLP, and the PO, which give distinct information about the scene being imaged.

We next study the performance of the various PO estimators in white and colored noise.

A. Polarization Orientation Imaging in White Noise

The CRLB for estimation of β in white Gaussian noise can be shown to be

$$\mathrm{var}\{\hat{\beta}\} \geq \frac{2\sigma^2}{N{I_{\mathrm{bal}}}^2} = \frac{1}{N\eta}, \tag{26}$$

where η represents the SNR; i.e., $\eta = {I_{\mathrm{bal}}}^2/2\sigma^2$, where σ is the noise variance.

However, it has been found that there does not exist a MVU phase estimator that attains the CRLB for this case in white Gaussian noise.[12] This result is applicable to our problem too. But the MLE of phase exists because of the invariance property and is given approximately by[12] [from Eqs. (18) and (19)]

$$\hat{\beta}_{\mathrm{MLE}} = \arctan\left(\frac{\hat{I}_{\mathrm{bal}} \sin \beta_{\mathrm{MVU}}}{\hat{I}_{\mathrm{bal}} \cos \beta_{\mathrm{MVU}}}\right) = \arctan\left[\frac{\sum_{n=0}^{N-1} I_r(n)\cos(4\pi n/M)}{\sum_{n=0}^{N-1} I_r(n)\sin(4\pi n/M)}\right], \tag{27}$$

where M is the periodicity of the rotating polaroid and N is the number of data points available for analysis.

$\hat{\beta}_{\mathrm{MLE}}$ also corresponds to the phase of the complex DFT coefficient that corresponds to the frequency of the sinusoid. Because the PMI estimator obtains the DFT coefficient from which we can estimate the phase of the sinusoid, we conclude that the PMI phase estimator obtains the MLE of phase. The asymptotic variance of the PMI phase estimator has been shown to reach the CRLB given by Eq. (26).[12] The transformation function used to estimate the phase is noninvertible; thus $\hat{\beta}_{\mathrm{MLE}}$ actually maximizes a modified likelihood function.[12]

B. Polarization Orientation Imaging in Colored Noise

The CRLB for estimating β in colored noise can be shown to be

$$\mathrm{var}\,\hat{\beta} \geq \frac{a_{11}a_{22} + (a_{11}a_{23} - a_{12}a_{13})\,\sin 2\beta - {a_{12}}^2\cos^2\beta - {a_{13}}^2\sin^2\beta}{{I_{\mathrm{bal}}}^2 \det(\mathbf{A})}, \tag{28}$$

where $\mathbf{A} = \mathbf{H}^T\mathbf{C}^{-1}\mathbf{H}$ [see Eq. (15) for the meaning of $\mathbf{H}$ and $\mathbf{C}$].

It can be observed that the CRLB for β depends not only on the amplitude of the sinusoid I_{bal} (or the SNR) as in the case of white noise but also on β itself. However, the dependence on β was found to be weak, essentially making the CRLB invariant to β.

As in the case of white noise, the PMI estimate of phase is given by the argument of the complex discrete Fourier transform coefficient that corresponds to the frequency of the sinusoid. For the MLE, we need to use Eq. (27). Because of the asymptotic properties of the MLE, the estimator achieves the bound given in Eq. (28) when a large number of data points are available for analysis. Once again, $\hat{\beta}_{\mathrm{MLE}}$ actually maximizes a modified likelihood function, as in the case of white noise.

C. Results from Monte Carlo Simulations

Figures 3(a) and 3(b) show the performance of the PMI estimator and the APES in white and AR1 noise, respectively. As was mentioned above, the PDI estimator is incapable of estimating this parameter. We can observe that the PMI estimator performs better than the APES in both white Gaussian noise and AR1 noise. It should also be observed that the PO estimates for colored noise seem meaningful only at values of SNR above 5 dB. Hence it should be kept in mind that the PO imaging is useful only when SNRs are relatively high. F3

Here we conclude our analysis of the estimators used for estimating the various visualization parameters.

6. Novel Color-Based Rendition Scheme

In previous sections we introduced three visualization parameters for polarization-based direct imaging schemes. We studied the various estimators for each of these parameters and their characteristics. In all the schemes discussed, the visualization parameters are finally rendered as gray-scale images. If we want to study all the visualization parameters of a scene, we need to study three different images. In this section we propose a new scheme for rendering the polarization information whereby the visualization parameters are intuitively mapped to various aspects of a color image, giving a holistic view of the scene.

The information on polarization magnitude inherently has the notion of intensity, i.e., the intensity of polarized light. The DOLP signifies the purity of the polarized radiation and parallels the idea of saturation in color images. In color images, the greater the purity of a color, the higher will be the saturation. The polarization-orientation parameter distinguishes different states of linear polarization and is akin to different hues in a scene. Thus the three visualization parameters correspond intuitively to the parameters of a normal color image and hence can be rendered so. We next show some illustrative simulation results.

We synthesized 32 images of size 160 × 100 pixels to study the suitability of fusing the visualization parameters. The data at each pixel location were synthesized according to Eq. (4). We considered the noise

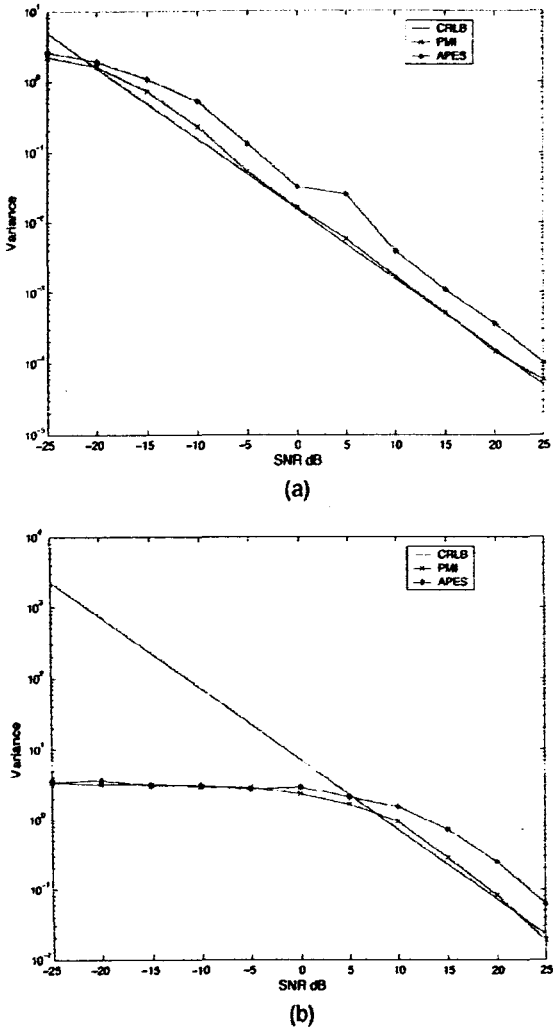

Fig. 3. Performance of PO estimators. (a) Variance of PO estimators in white noise. (b) Variance of PO estimators in AR1 noise.

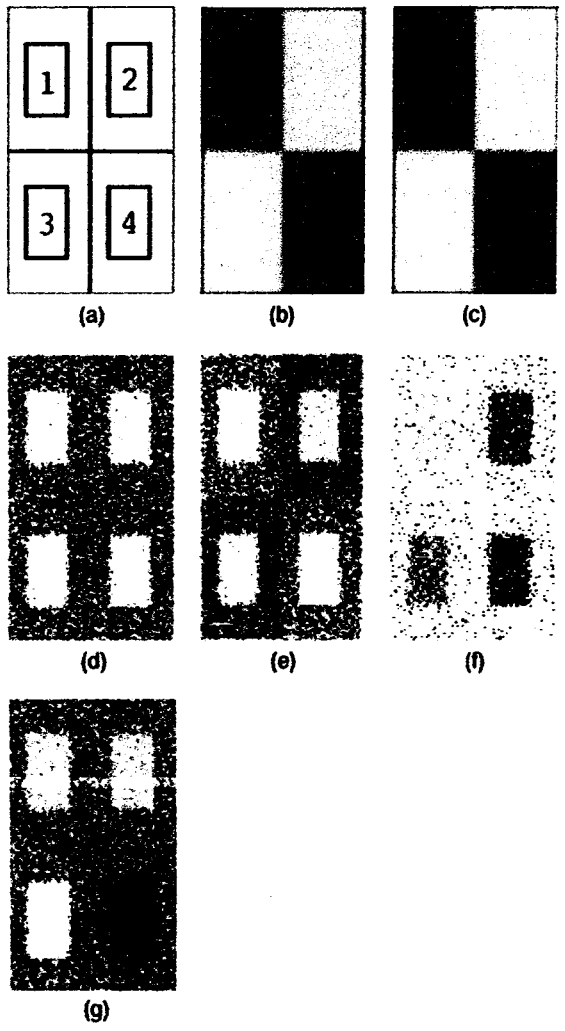

Fig. 4. Result of fusing the visualization parameters. (a) Break-up of synthetic images. (b) A representative of the 32 images in the series. (c) Result of histogram equalizing (b). (d) PMI N magnitude estimation result. (e) PMI N DOLP estimation results. (f) PMI N PO estimation result. (g) Result of fusing (d), (e) and (f).

to be white Gaussian for these simulations, but the results for colored noise will be no different.

The synthesized images were divided into four quadrants, as shown in Fig. 4(a). The value of I_{scat} was chosen to be 170 in quadrants 1 and 4, and 240 in quadrants 2 and 3. Within each quadrant we chose rectangular subregions of size 40 × 30, as shown in Fig. 4(a). The value of I_{bal} was chosen to be 0 at all locations, except in the subregions. It was chosen to be 0.2 in the subregions of every quadrant, thus giving a DOLP of 0.0011 in the subregions of quadrants 1 and 4 and of 0.0008 in the subregions of quadrants 2 and 3. Before the addition of noise, the images were blurred by use of a Gaussian mask of size 9 × 9 to simulate blurring that is due to the optical elements. Though we have not analyzed the nature of the blur in an actual experimental setup, we use the Gaussian blur only to study the probable effect of blurring.

To the blurred data we added white Gaussian noise at every pixel location across images. The noise at each pixel location had a variance of 0.05, leading to a SNR of nearly −4 dB in all the subregions. The reason for choosing such small values for I_{bal} and the DOLP is to show the robustness of the polarization-based imaging techniques even at relatively low SNRs, when the individual images in the series do not convey any visual information about polarization by themselves. The information becomes evident only after processing.

The phases of the sinusoids in the subregions were chosen to be $2\pi/9$, 0, $5\pi/18$, and $15\pi/9$. The phases were chosen arbitrarily to illustrate the feasibility of rendering the polarization information as color images and are not related to the processing itself. We used the PMI estimator to estimate the various visualization parameters, as the PDI scheme is incapable of estimating the phase information. The parameters can also be obtained with the APES.

Figure 4(b) shows a representative image of the set of 32 images that looked nearly alike. Figure 4(c)

Table 1. Elements of Experimental Setup Shown in Fig. 5

Scattering medium	Polystyrene spheres of 2.97 μm diameter dispersed in distilled water
Source	10 mW, 632.8 nm He–Ne laser source
Detector	Intensified CCD
Images	Gray scale (256 levels); size, 240 × 320
Scattering mean free path length, l_s	334.7 μm
Transport mean free path length, l^*	1760 μm
Optical thickness, τ	5.68
Average SNR of a time series	−1.2 dB
Periodicity of the analyzer, M	16
Initial phase, β	$\approx\pi/2$

shows the histogram equalized version of the representative image. As we can observe, we do not find any discernible difference among the subregions, but we find a difference in the gray scales of the four quadrants. The same was true for other images in the series too. Figure 4(d) shows the result of analyzing the magnitude of polarization. It can be observed that the four subregions have the same information on magnitude of polarization. Figure 4(e) shows the result of DOLP analysis wherein we can observe a slightly higher DOLP in the subregions of quadrants 1 and 4 compared with those of quadrants 2 and 3. As the magnitude of the DOLP is small, perhaps we could not have expected a drastically different result. Figure 4(f) shows the result of PO analysis. The subregions are clearly distinguishable from the background. However, only the subregion of the first quadrant stands apart uniquely from the others. Thus, though it is attractive to use POI to differentiate regions with polarization information, it is not easy to differentiate the PO from these results.

Figure 4(g) shows the result of fusing all the visualization parameters into a color image, as explained above. The color image clearly shows the POs of the subregions. Keen observation also shows the lower saturation levels of the colors in quadrants 2 and 3 compared with the colors of quadrants 1 and 4. This corresponds to the difference in the DOLP of these subregions. It is clear that rendering the parameters as a color image can provide better insight into the various polarization parameters than can rendering them as gray-scale images.

7. Experimental Results

We conducted experiments to obtain shadowgrams of an opaque object immersed in calibrated solutions containing polystyrene microspheres dispersed in water. The experimental setup used was similar to the one described in Ref. 5. The parameters of the experiment from which the data were obtained are T1 given in Table 1. We observed that with microspheres

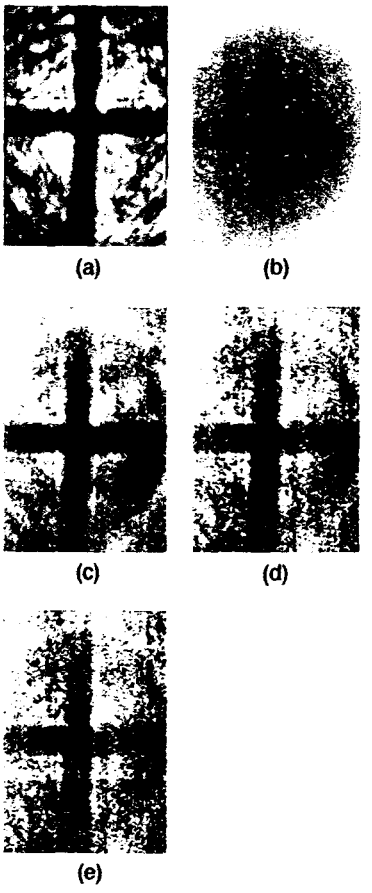

Fig. 5. Experimental results. Details of the experimental setup are given in Table 1. (a) Actual object. (b) Unprocessed image. (c) PDI result. (d) PMI result. (e) PES result.

of 2.97 μm diameter we could image an optical thickness of as much as 6.77, whereas we could image an optical thickness of as much as of 40 in samples containing polystyrene beads of 0.11 μm diameter. A result obtained from one of the data sets is shown in Fig. 5. Figure 5(a) shows the shadow of the object F5 without scattering. Figure 5(b) shows a representative image in the series of images acquired. Figures 5(c), 5(d), and 5(e) show the polarization intensity imaging results obtained by processing 16 images recorded by use of the PDI, PMI, and APES schemes, respectively. One can easily observe the superiority of the PDI scheme by comparing the results, which endorse our theoretical observations.

8. Potential Application of Polarization Orientation Imaging

We now show a potential application of POI, using the estimates obtained by the PMI estimator from one of our experiments. As we saw above, POI is useful only if the SNR is relatively high or if a large number of data points are available for analysis. However, for illustrating the advantages of POI, we report positive results from an experiment that used

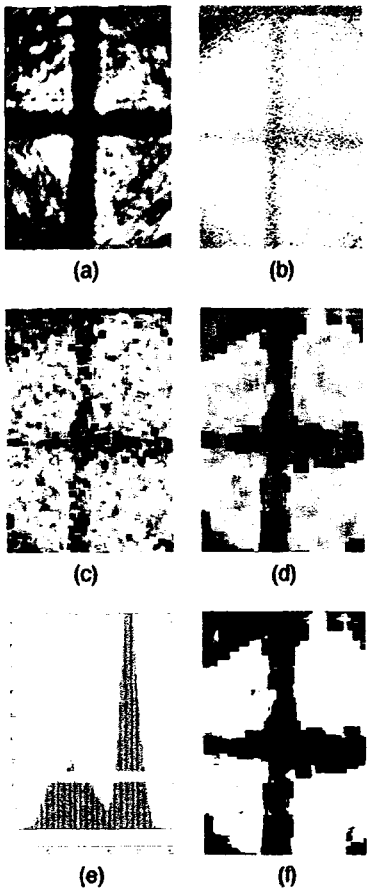

Fig. 6. Segmentation of a POI result. (a) Image without scattering. (b) Result of PMI POI; $N = 512$. (c) 9×9 block processing result. (d) 15×15 block processing result. (e) Histogram of (d). (f) Result of segmenting (e).

512 images of a data set, albeit with a relatively low SNR (≈ -8 dB).

If a single linearly polarized source is used, then ideally the region not blocked by the object should yield the same phase information at every pixel location. Depending on the SNR, the values of estimated phase will fluctuate only slightly about the mean value. However, wherever the object blocks the ballistic light, the phase estimation should yield random results. Thus the correlation in the resultant POI estimates of neighboring pixels in regions receiving the ballistic component should be much higher than those of regions blocked by the object. As we show, this information can be exploited in segmenting the image into target and background regions. This sort of segmentation and, hence, POI is useful in defense-related applications. Moreover, the analogy can be extended to regions that contain different POs also.

For testing the validity of our hypothesis, we considered rectangular blocks of sizes 9×9 and 15×15 centered about every pixel location excluding the boundary pixels. We cross correlated the data in every block with blocks around the adjacent eight neighbors and took the maximum of the cross-correlation values as the result for that pixel. We finally plotted these results as an image. Figure 6 gives these results. Instead of taking the maximum of the correlation values, we also took the average of the correlation values and observed similar results. We found that the resultant images had histograms that clearly showed two modes, compared with the PII and DOLP results that could not clearly distinguish the object and the background. This information can be used to segment the images into regions that correspond to the hidden object and the background.

Figure 6(a) shows the image of the object without scattering. Figure 6(b) shows the POI result obtained from 512 images of a data set. Figure 6(c) shows the result obtained from the cross-correlation technique described above when the block size was 9×9. Figure 6(d) shows the result with blocks of size 15×15. Figure 6(e) shows a histogram of the image in Fig. 6(d). Figure 6(f) shows the result of thresholding Fig. 6(d) at a value lying in the valley between the two modes of the histogram. As we can observe, though the exact boundary of the object is not visible we can get an idea of the presence of a hidden object in the medium. This sort of information is useful in many defense-related applications. The processing described above can be followed by morphological operations to get better results.

Though we can segment polarization intensity and DOLP images, the POI segmentation is robust when the variation in the estimates of phase is smaller than the variation in I_{bal} and I_{scat}. Unlike phase, I_{bal} and I_{scat} can have larger distributions. This is the advantage of using POI results for segmentation. The segmentation scheme discussed above is fairly rudimentary. We can perhaps develop many more such algorithms, using PII, DOLP, and POI results.

9. Conclusions

We have detailed the framework for analyzing continuous-wave, direct, polarization-based imaging schemes. With small modifications, most of the analysis can be extended to include circular polarization based imaging schemes. We have derived bounds on the performance of most of the imaging schemes and have compared them by using the framework developed. We have brought into this framework the various visualization parameters, thus being able to show the commonalities and differences among the imaging schemes. A novel color based rendition scheme and application of the newly introduced polarization orientation imaging for segmentation have been introduced, showing the possible enhancements and applications of these imaging schemes.

An experiment was conducted with an incoherent white-light source to study the feasibility of using ordinary sources for polarization-based imaging. The experiment verified such a possibility by yielding encouraging results. Some enhancements were incorporated into the analysis part of the imaging schemes by bootstrapping and data chunking.[15] These methods provided a marginal improvement over the existing schemes and hence have not been reported in this

study. In short, we have been able to leverage the strength of estimation-theoretic concepts in studying polarization-based imaging schemes.

References

1. J. C. Hebden, S. R. Arridge, and D. T. Delpy, "Optical imaging in medicine. I. Experimental techniques," Phys. Med. Biol. **42**, 825–840 (1997).
2. R. S. Umesh, A. G. Ramakrishnan, R. Srikanth, and R. Hema, "Estimation theoretic framework for comparing polarization based, continuous-wave direct imaging schemes," in *International Conference on Signal Processing and Communications* (**name of publisher,** 2004), pp. 535–539. AQ: K
3. M. P. Rowe, E. N. Pugh, Jr., J. S. Tyo, and N. Engheta, "Polarization-difference imaging: a biologically inspired technique for observation through scattering media," Opt. Lett. **20**, 608–610 (1995).
4. J. S. Tyo, M. P. Rowe, E. N. Pugh, Jr., and N. Engheta, "Target detection in optically scattering media by polarization-difference imaging," Appl. Opt. **35**, 1855–1870 (1996).
5. R. Hema and N. Andal, "Two-dimensional imaging through turbid media using a continuous wave light source," Opt. Commun. **154**, 255–260 (1998).
6. O. Emile, F. Bretenaker, and A. Le Floch, "Rotating polarization imaging in turbid media," Opt. Lett. **21**, 1706–1708 (1996).
7. C. F. Bohren and D. R. Huffman, *Absorption and Scattering of Light by Small Particles* (Wiley, 1998).
8. W. S. Bickel and W. M. Bailey, "Stokes vectors, Mueller matrices, and polarized scattered light," Am. J. Phys. **53**, XX–XX (1985). AQ: L
9. S. Huard, *Polarization of Light* (Wiley, 1997).
10. C. Brosseau, *Fundamentals of Polarized Light—A Statistical Optics Approach* (Wiley, 1998).
11. J. G. Walker, P. C. Y. Chang, and K. I. Hopcraft, "Visibility depth improvement in active polarization imaging in scattering media," Appl. Opt. **39**, 4993–4941 (2000).
12. S. M. Kay, *Fundamentals of Statistical Signal Processing: Estimation Theory* (Prentice-Hall, 1993).
13. P. Stoica, H. Li, and J. Li, "Amplitude estimation of sinusoidal signals: survey, new results, and an application," IEEE Trans. Signal Process. **48**, 338–352 (2000).
14. G. M. P. van Kempen and L. J. van Vliet, "Mean and variance of ratio estimators used in fluorescence ratio imaging," Cytometry **39**, 300–305 (2000).
15. R. S. Umesh, "Algorithms for processing polarization-rich optical imaging data," M. S. thesis (Indian Institute of Science, Bangalore, 2004), http://etd.ncsi.iisc.ernet.in/handle/2005/96.